Characterization of a Lacustrine Shale Reservoir and the Evolution of its Nanopores: A Case Study of the Upper Cretaceous Qingshankou Formation in the Songliao Basin, Northeastern China

ZHANG Xu[1,2,3,4], LIU Chenglin[1,2,*], LI Bing[1,2], WU Linqiang[5], GUI Herong[3,*], WANG Ziling[1,2], ZHANG Zhihui[1,2] and LIANG Dexiu[1,2]

[1] *State Key Laboratory of Petroleum Resource and Prospecting, China University of Petroleum, Beijing 102249, China*

[2] *College of Geosciences, China University of Petroleum, Beijing 102249, China*

[3] *National Engineering Research Center of Coal Mine Water Hazard Controlling（Suzhou University）, Suzhou, Anhui, 234000, China*

[4] *Geological Exploration Technology Institute of Anhui Province, Hefei, Anhui, 230031, China*

[5] *Development and Research Center, China Geological Survey, Beijing 100037, China*

Abstract: The Songliao Basin is one of the most important petroliferous basins in northern China. With a recent gradual decline in conventional oil production in the basin, the exploration and development of unconventional resources are becoming increasingly urgent. The Qingshankou Formation consists of typical Upper Cretaceous continental strata, and represents a promising and practical replacement resource for shale oil in the Songliao Basin. Previous studies have shown that low-mature to mature Qingshankou shale mainly preserves type I and type II_1 organic matter, with relatively high total organic carbon (TOC) content. It is estimated that there is a great potential to explore for shale oil resources in the Qingshankou Formation in this basin. However, not enough systematic research has been conducted on pore characteristics and their main controlling factors in this lacustrine shale reservoir. In this study, 19 Qingshankou shales from two wells drilled in the study area were tested and analyzed for mineral composition, pore distribution and feature evolution using X-ray diffraction (XRD), scanning electron microscopy (SEM), low-pressure nitrogen gas adsorption (N_2-GA), and thermal simulation experiments. The XRD results show that clay, quartz, and feldspar are the dominant mineral constituents of Qingshankou shale. The clay minerals are mostly illite/smectite mixed layers with a mean content of 83.5%, followed by illite, chlorite, and kaolinite. There are abundant deposits of clay-rich shale in the Qingshankou Formation in the study area, within which many mineral and organic matter pores were observed using SEM. Mineral pores contribute the most to shale porosity; specifically, clay mineral pores and carbonate pores comprise most of the mineral pores in the shale. Among the three types of organic matter pores, type B is more dominant the other two. Pores with diameters greater than 10 nm supply the main pore volume; most are half-open slits and wedge-shaped pores. The total pore volume had no obvious linear relationship with TOC content, but had some degree of positive correlation with the content of quartz + feldspar and clay minerals respectively. However, it was negatively correlated with carbonate mineral content. The specific surface area of the pores is negatively related to TOC content, average pore diameter, and carbonate mineral content. Moreover, it had a somewhat positive correlation with clay mineral content and no clear linear relationship with the content of quartz + feldspar. With increases in maturity, there was also an increase in the number of carbonate mineral dissolution pores and organic matter pores, average pore diameter, and pore volume, whereas there was a decrease in specific surface area of the pores. Generally, the Qingshankou shale is at a low-mature to mature stage with a TOC content of more than 1.0%, and could be as thick as 250 m in the study

* Corresponding author. E-mail: liucl@cup.edu.cn (LIU Chenglin); hrgui@163.com (GUI Herong).

This article has been accepted for publication and undergone full peer review but has not been through the copyediting, typesetting, pagination and proofreading process, which may lead to differences between this version and the Version of Record. Please cite this article as doi: 10.1111/1755-6724.14328.

area. Pores with diameters of more than 10 nm are well-developed in the shale. This research illustrates that there are favorable conditions for shale oil occurrence and enrichment in the Qingshankou shale in the study area.

Key words: lacustrine shale, Upper Cretaceous, pore structure, pore evolution, Songliao Basin

E-mail: xuzhangcags@163.com

1 Introduction

In recent years, unconventional resources such as shale oil and gas have changed the structure of the global energy economy. These resources are also being developed in China, especially with the commercial development of shale gas in the Sichuan Province (Liu et al., 2012; Bahadur et al., 2014; Zhang et al., 2015; Zhang et al., 2015a; Xue et al., 2016; Yang et al., 2016; Hao et al., 2017). Undoubtedly, pore characteristics play important roles in shale oil and gas exploration as well as development (Guo et al., 2015; Yang et al., 2015b; Zhang et al., 2015b; Wang et al., 2016a; Wang et al., 2014, 2016b; Chen et al., 2017). Much research has been published on fracture and micropore types, distribution, and morphology, as well as the factors that control shale development (Huang et al., 2013a, b; Chen et al., 2015; Chen et al., 2016; Cao et al., 2016; Clarkson et al., 2016; Ran et al., 2016; Wang et al., 2017). Slatt and O'Brien (2011) defined and identified porous floccules, organopores, fecal pellets, fossil fragments, intraparticle pores, microchannels, and microfractures present in the Barnett and Woodford shales. In addition to microfractures and organoporosity, clay flocculation has the greatest potential to create porosity. Pores in shale were classified as intraparticle, interparticle, intercrystal, and organic pores according to their relationship with the mineral matrix and organic matter (Loucks et al., 2012; Jiang et al., 2014; Zhang et al., 2015a).

For pore distribution and the factors controlling its development in shale reservoirs, published experimental and observational studies have indicated that these phenomena are related to the sedimentary environment, mineral composition, content as well as types of organic matter, maturity, diagenesis, and preservation (Locks et al., 2007, 2012; Slatt and O'Brien, 2011; Jiang et al., 2014; Suárez-Ruiz et al., 2016). Loucks et al. (2007) suggested that a deep-water, euxinic foreland basin well below storm-wave base is suitable for preserving organic matter, creating rich source rock, and along with abundant framboidal pyrite. Pore morphologies and pore sizes are clearly related to the mineral fabric, and moreover, large pores with internal faceted crystal morphology exist in recrystallized calcite clasts, and pores in the clay-rich matrix and nannofossils are smaller (Klaver et al., 2012).

Many published reports suggest that organic matter maturity corresponds with pore development in shale (Loucks et al., 2012; Huang et al., 2013a; Jiang et al., 2014). For an average total organic carbon (TOC) content of 6.41 wt.% (mass), the volume percent of TOC is about 12.7 vol.%, and approximately 4.3 vol.% porosity is created from immaturity to the dry-gas window because of the decomposition of organic matter (Jarvie et al., 2007). Mastalerz et al. (2012) demonstrated that micro- and mesopore volumes are correlated with organic matter content in the early mature Upper Devonian–Mississippian shale. With increasing thermal evolution, more pores are generated in organic matter and some mineral pores are created by organic acid dissolution (Huang et al., 2013a; Jiang et al., 2014). Bahadur et al. (2015) established that total porosity decreases with maturity whereas it increases somewhat in post-mature samples. However, there are also some other considerations. Factors such as the composition of the organic matter, development of complex porosity, and preservation, not only thermal maturity alone, need to be considered in predicting porosity in organic matter (Curtis et al., 2012). Organic pores with similar sizes and shapes have been identified in both immature and mature organic-rich mudstones and were not likely related to thermogenic hydrocarbon generation (Fishman et al., 2012). Organic and mineral pores both play important roles in various shales. For organic-poor and clay-rich shale, water-accessible sheet-like pores within clay aggregates provide dominantly nano-sized pores. Nevertheless, bubble-like organophilic pores in kerogen dominate organic-rich samples (Gu et al., 2015). In addition, organic and mineral pores contribute in various ways to porosity and specific surface area. King et al. (2015) reported pores of a broad power law distribution with inter/intragrain mineral porosity, and small (< 3 nm) pores housed in the organic matrix that constitute about one-third of the total porosity in gas shale reservoir rocks. Bahadur et al. (2014) showed that the porosity and

specific surface area of Cretaceous shale are dominated by the contributions of meso- and micropores. There is no correlation between total porosity and mineral components. Zhang et al. (2015c) revealed that shale porosity has no correlation with quartz and clay ratios, but correlates well with TOC content. Microporous organic matter in high-maturity shale provides a large internal surface area.

Recently, there has been insufficient research on shale gas and shale oil within lacustrine shale (Wang et al., 2015; Han et al., 2018). The Songliao Basin is one of the most important petroliferous basins in China, and several high-quality oil shale mines have been developed in its southeastern uplift unit (Liu et al., 2014a). With a gradual decline in conventional oil production, the exploration and development of unconventional resources, especially shale oil and gas, in the basin are becoming increasingly important. The Qingshankou Formation consists of typical Upper Cretaceous continental sedimentary strata and includes very thick shale depositions in the study area. The Qingshankou shale mostly preserves type I or type II_1 organic matter with high TOC content; the organic matter is at a low-mature to mature stage (Liu et al., 2014a；Liu et al., 2014b；Li et al., 2015). Although the Songliao Basin has great potential for shale oil and gas exploration, there is still not enough systematic research on shale reservoir characteristics and the controlling factors of the shale reservoir (Bechtel et al., 2012; Huang et al., 2014; Liu et al., 2014a; Dong et al., 2015). Therefore, research related to the features of the Qingshankou shale reservoir are sorely needed for shale oil exploration and development in the future.

2 Geological Settings

The Songliao Basin, a typical large Mesozoic–Cenozoic sedimentary basin in northeastern China, is characterized by a dual structure of faults and depressions (Shu et al., 2003). It is divided into six tectonic units: the southwestern, southeastern, and northeastern uplifts, central depression, western slope, and northern pitching (Wang et al., 2015) (Fig. 1). It underwent four major tectonic evolution events: thermal doming, rifting, depression, and structural inversion. Paleozoic metamorphic, volcanic, and magmatic rocks formed the basement of the basin, which is overlain by Jurassic, Cretaceous, and Cenozoic sedimentary rocks (Wang et al., 2013). Guo et al. (2012) divided the Cretaceous strata into two different filling sequences, of which the upper segment contains abundant hydrocarbon and oil shale deposits.

The Qingshankou Formation (K_2qn) consists of Upper Cretaceous continental layers representative of those in the Songliao Basin. They were deposited when the Songliao paleo-lake expanded continuously with an increasing sedimentary area; the Qingshankou Formation is in conformable and disconformable contact with the underlying Quantou Formation and can be divided into three members from bottom to top (Zhai and Ding, 1993). During the sedimentary period of the first member (K_2qn_1), the paleo-lake reached its greatest extent; this is when a set of dark mudstones and shales with high TOC content and abundant ostracod fossils was deposited in the Qingshankou Formation. Moreover, because of the semi-deep-lake and deep-lake paleoenvironment, the dark mudstone that was deposited in the central and southern Songliao Basin were more than 100 m thick. The sedimentation of the second and third members of the Qingshankou Formation (K_2qn_2 and K_2qn_3) occurred as the paleo-lake began to shrink, and most deposits were mudstone, siltstone, argillaceous siltstone, and silty mudstone. The mudstone, mostly gray, celadon, and dark gray in color, contains large quantities of ostracods, conchostracans, and plant debris; some mudstones even formed fossil-rich layers ranging from 2 to 30 cm thick. At the time of deposition, the central and southern parts of the Songliao Basin existed in a shore-shallow lake and prodelta sedimentary environment, corresponding with dark gray mudstone more than 500 m thick, with several calcareous siltstone and ostracod layers (Zhuo et al., 2007).

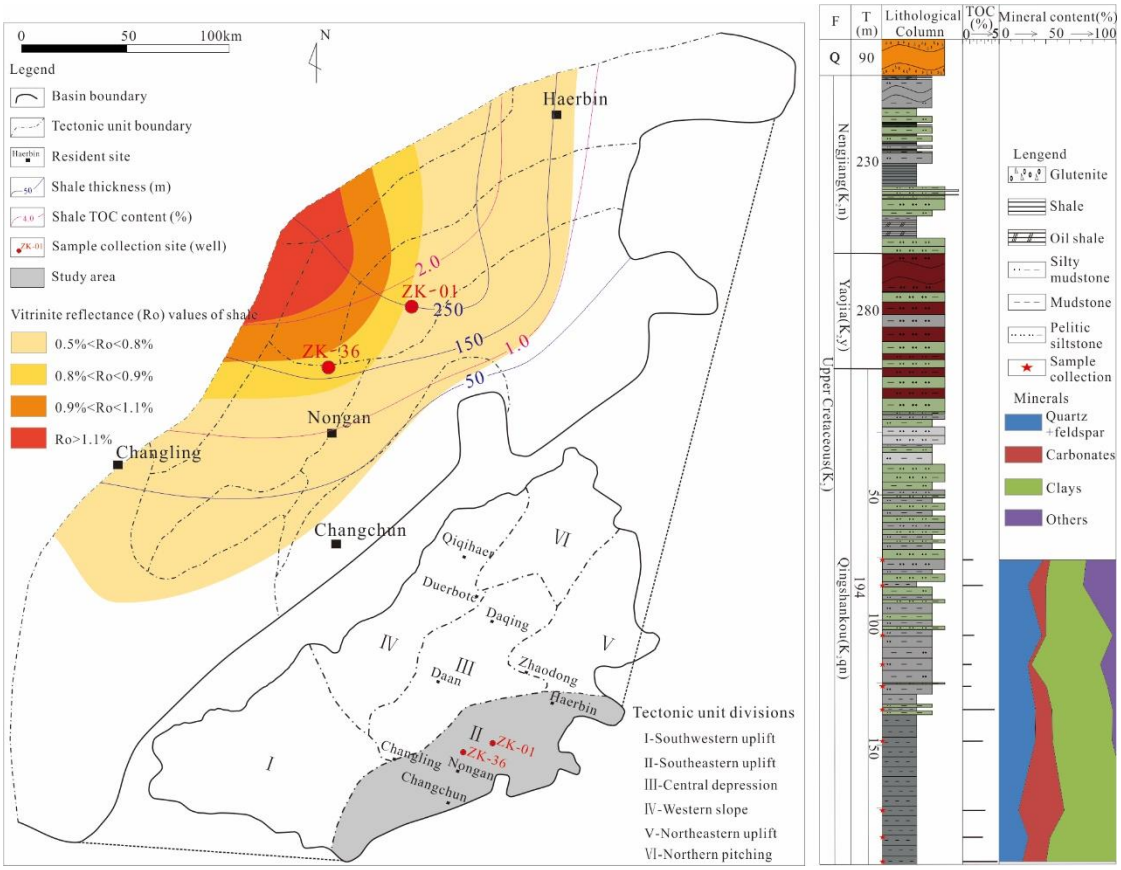

Fig. 1. The tectonic elements of the Songliao Basin and shale distribution of the Qingshankou Formation in the southeastern uplift. A comprehensive stratigraphic column and the TOC and mineral content of the shales were measured from well ZK-36 drilled in the southeastern uplift. F = Formation; T = Thickness. Some of the units and shale characteristics were modified by Shu et al. (2003) and Wang et al. (2015).

During the deposition of K_2qn_1, redox conditions in the bottom water fluctuated from oxic–dysoxic to euxinic–anoxic and oxic–dysoxic again; the latter was the most important factor in the formation of hydrocarbon source rocks in the Songliao Basin (Wang et al., 2013). Huang et al. (2013a, b) presented five types of pores in Qingshankou shale from the Songliao Basin, including matrix intercrystal, organic, dissolution, intergranular, and intracrystal pores, and micron- to nano-sized microfissures. The organic matter, illite, and pyrite content in the shale have positive correlations with pore volume; an increase of these contents would also lead to the increase of the amount and size of pores. However, the chlorite, quartz, calcite, and anorthose contents show negative correlations with pore volume. The micropores in source rocks are not affected by kaolinite. Huo et al. (2012) suggested that the hydrocarbons that remained in the source rocks, which belong to the first member of the Qingshankou Formation in the northern Songliao Basin, was mainly absorbed by organic matter and stored in pores. Source rocks with high organic matter content are more favorable for petroleum expulsion, and require relatively lower maturity to generate hydrocarbons than source rocks with low TOC contents. Nevertheless, when TOC content is lower than 0.4%, petroleum expulsion cannot occur. Wang et al. (2015) suggested that most pores are mesopores or micropores less than 50 nm in diameter in the first member of the Cretaceous Qingshankou Formation (K_2qn^1) in the northern part of the Songliao Basin. Pore volume has no apparent correlation with clay content. A weak negative correlation is presented between total pore volume and carbonate content. Nano-sized pores are well-developed in the shales, with Ro more than 1.0%, and are positively correlated with TOC content. However, when the organic matter maturity is less than 1.0%, pores are poorly developed and the pore volume is not correlated with maturity or TOC content. In addition, the degree of the development of pores showed no obvious relationship with clay or carbonate contents. The statistics on S_1 content and pore volumes with different pore sizes showed that shale oil mainly existed in pores with diameters greater than 40 nm.

Overall, Upper Cretaceous Qingshankou shale is widely developed in the Songliao Basin, and thickness and maturity increase from the periphery to the center of the basin. As the southernmost location of the Songliao Basin, the southeastern uplift has great shale oil resource potential; the

Qingshankou shale it could exceed 250 m in thickness, with low-mature to mature maturity. In addition, the TOC content of the shale is generally over 1.0% (Fig. 1).

3 Samples and Methods

The samples of the Qingshankou shale used in this research were collected from wells ZK-01 and ZK-36 in the southeastern uplift of the Songliao Basin (Fig 1). The TOC and mineral contents and pore size distribution and morphology were investigated to describe the present characteristics of the shale in the study area. Some samples of low maturity shale were artificially heated to 380 ℃ and 460 ℃ to allow observation of the pore morphology and testing of the pore size distribution, which could be helpful to study the evolution of pore characteristics as the shale went from low-maturity to maturity. The mineral content of 19 samples were tested using an X-ray diffraction (XRD) instrument (Lab XRD-6000), and data on their intensity in the 2θ range from −183° to −6° was collected at 0.002° intervals. We tested the TOC content of 16 samples using a carbon and sulfur analyzer (CS230HC) on 80−mesh samples, following the State Standard of the People's Republic of China (GB/T 19145-2003). Thermal simulation was completed utilizing a high temperature and pressure instrument (RML-1). Two samples were ground to powder and vacuumed in the instrument to be heated to 380 ℃ and 460 ℃ in 3 h. The temperature remained constant for 48 h after the setting temperature was reached. The mineral and pore morphologies were observed using scanning electron microscopy (SEM) (Quanta200F). The pore size distribution and structure of 15 samples were confirmed using a low pressure nitrogen gas adsorption instrument of (Micrometrics Tristar Ⅱ 3020). They were fitted into a 110 ℃ vacuum container to degas for approximately 14 h to remove moisture and other objects attached to the samples. The pore size distribution and specific surface area of the samples were computed using the Barrett−Joyner−Halenda (BJH) method and Brunauer−Emmett−Teller (BET) model, respectively. These tests were conducted at the State Key Laboratory of Petroleum Resource and Prospecting, China University of Petroleum (Beijing).

4 Results

4.1 Pore structure and distribution

4.1.1 Pore size distribution

Based on the pore classification scheme in Brunauer et al. (1940), the low−pressure nitrogen gas adsorption (N_2-GA) isotherms of 11 samples of the Qingshankou shale were categorized as type Ⅱ. At relatively low pressure, the adsorption curve rises slowly because of the filled micropores and fine mesopores. When the relative pressure is near $P/P_0 = 1$, the curve rises rapidly because of the adsorption of large meso- and macropores (Labani et al., 2013). Based on the adsorption curves with hysteresis loops classified by De Boer (Labani et al., 2013; Zhang et al., 2015a), the curves of the Qingshankou shale can be described as types B and C. These findings illustrate that the pores are mainly semi-open, e.g., slit- and wedge-shaped, pores because the hysteresis loop is relatively narrow at a relative pressure from 0.5 to 1.0 (Fig. 2). They also show that shales with similar mineral compositions have similar adsorption–desorption isotherm curves (Table 1, Fig. 2). The mineral content has an important influence on pore development in the shale. The relationship between pore volume and diameter is similar; pores with diameters of more than 10 nm contribute most to the pore volume (Fig. 3).

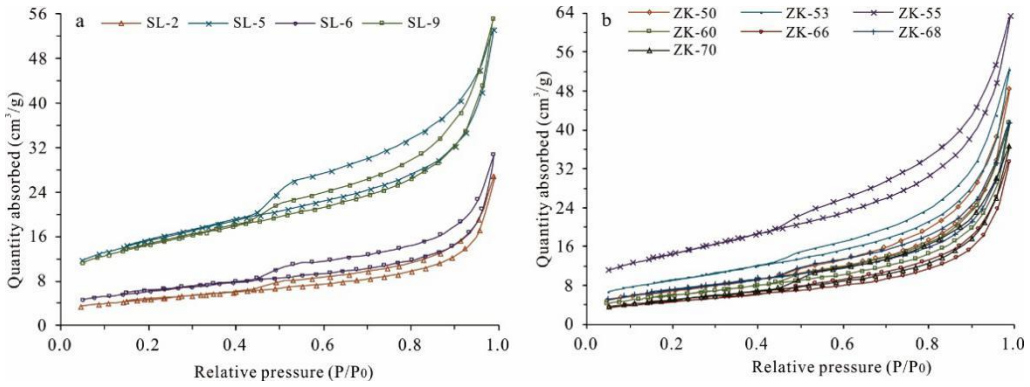

Fig. 2. Adsorption–desorption isotherms of the Qingshankou shales using N_2-GA.

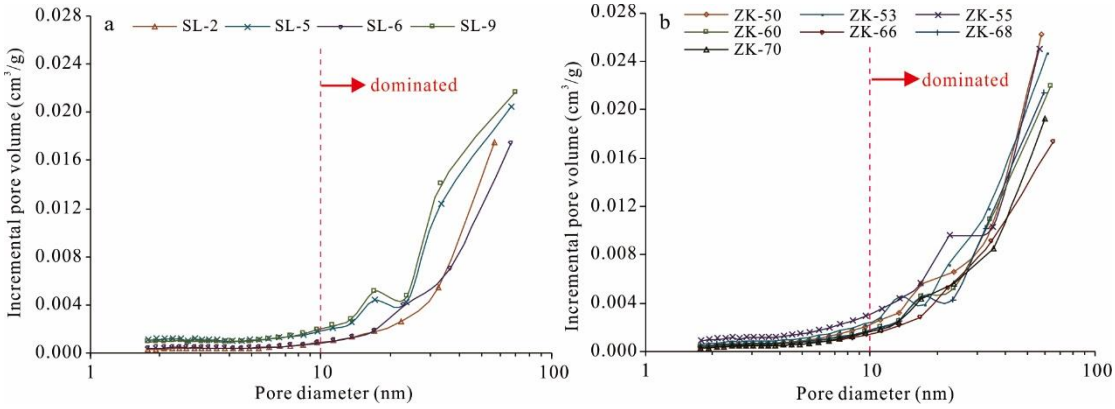

Fig. 3. Relationships between pore diameter and incremental pore volume of the Qingshankou shales by N_2-GA.

4.1.2 Pore volume and surface area

By using N_2-GA, the total pore volume and surface area of the shale samples were measured. The average BET surface area of 11 shale samples was 30.2 m^2/g, with range from 16.6 to 53.4 m^2/g. The total pore volume of the shale ranged from 0.038 to 0.087 cm^3/g, with an average of 0.063 cm^3/g (Table 2).

4.2 Pore morphology

4.2.1 Mineral pores

Based on the observation of mineral and pore morphology in the shale using SEM, intraparticle and interparticle pores were mainly identified in the clay, carbonate minerals, siliceous minerals, and pyrite. A large number of intraparticle pores with narrow wedge, triangular, and honeycomb shapes developed in the clay matrix, and their diameters varied from dozens to hundreds of nanometers (Fig. 4b, h, i, o). Some intraparticle and interparticle pores were related to carbonate minerals, such as calcite and dolomite. Jagged and oval intraparticle pores with diameters of dozens to hundreds of nanometers were observed in calcite, and most of them were formed by dissolution (Fig. 4a, e, g, n, p). The interparticle pores showed slit patterns with diameters of several hundreds to thousands of nanometers, and commonly developed at the edges of carbonate grains (Fig. 4d, i, l, m, n, p). In addition, there were some oval intraparticle pores in quartz (Fig. 4f) and jagged ones in feldspar (Fig. 4k). Pyrite framboids with many intraparticle pores generally developed in the shale (Fig. 4f), and some interparticle pores with diameters of several hundreds of nanometers occurred at the edges of pyrite (Fig. 4c, i, m, n).

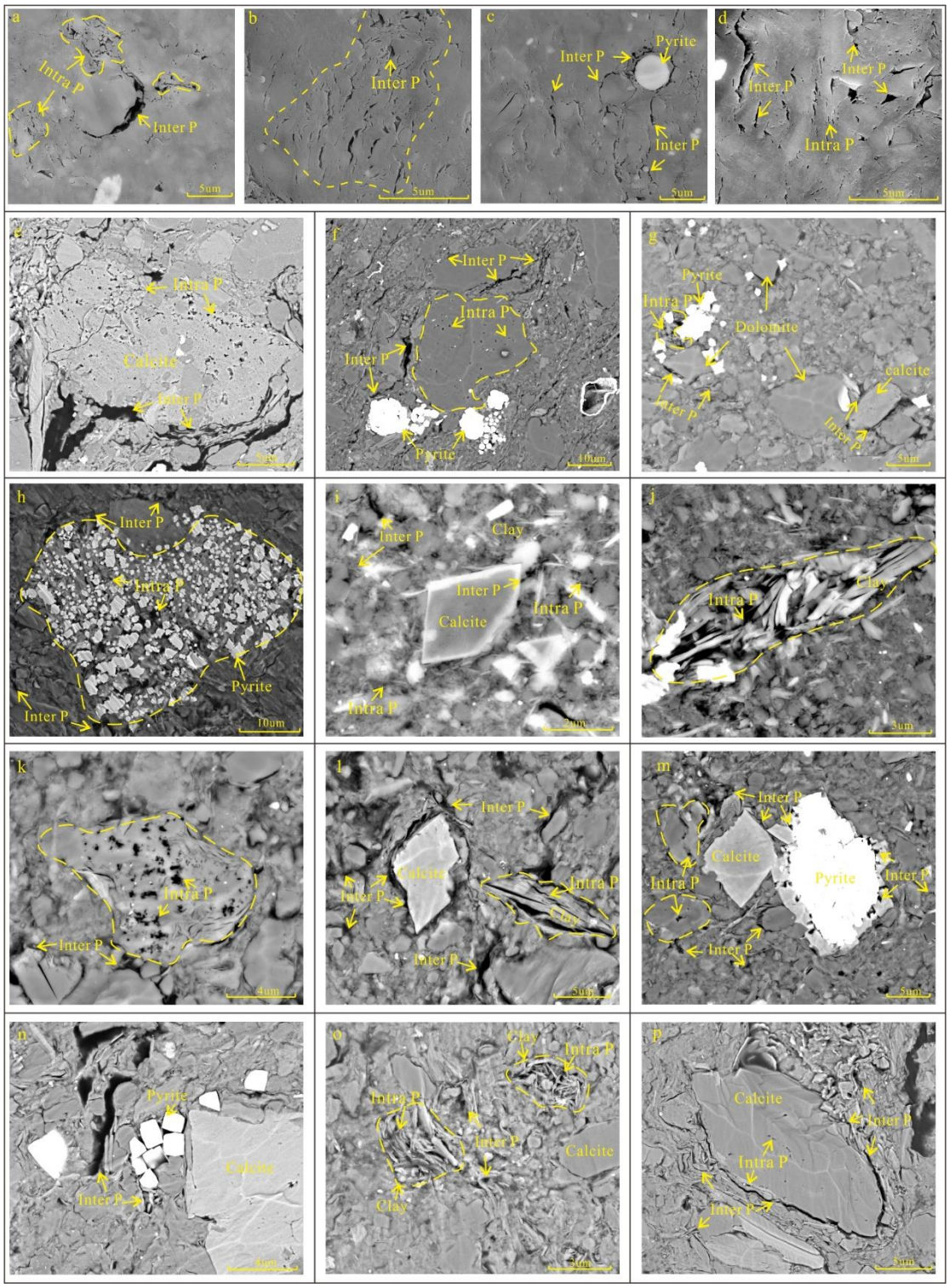

Fig. 4. Overview of mineral pores of the Qingshankou shale from the southeastern uplift in the Songliao Basin.

The samples of picture a - d were collected from well ZK-01. a = 307 m; b, c = 318 m; d = 349 m. The samples of picture e - p were collected from well ZK-36. e, f = 686 m; g, h = 736 m; i, j, k, l = 775 m; m, n = 787 m; o, p = 797 m. Interp P = interparticle pores, Intra P = intraparticle pores.

4.2.2 Organic matter pores

Based on the classification and identification of organic matter pores by Loucks et al. (2012),

Fishman et al. (2012), and Klaver et al. (2015), three types organic pores were observed and identified using SEM.

(1) Type A: The organic matter is irregular and scattered and mixed with inorganic minerals such as clay and calcite. Few pores are developed within the organic matter and most of the serrated pores are on the edges of the organic matter (Fig. 5a, b, c, d).

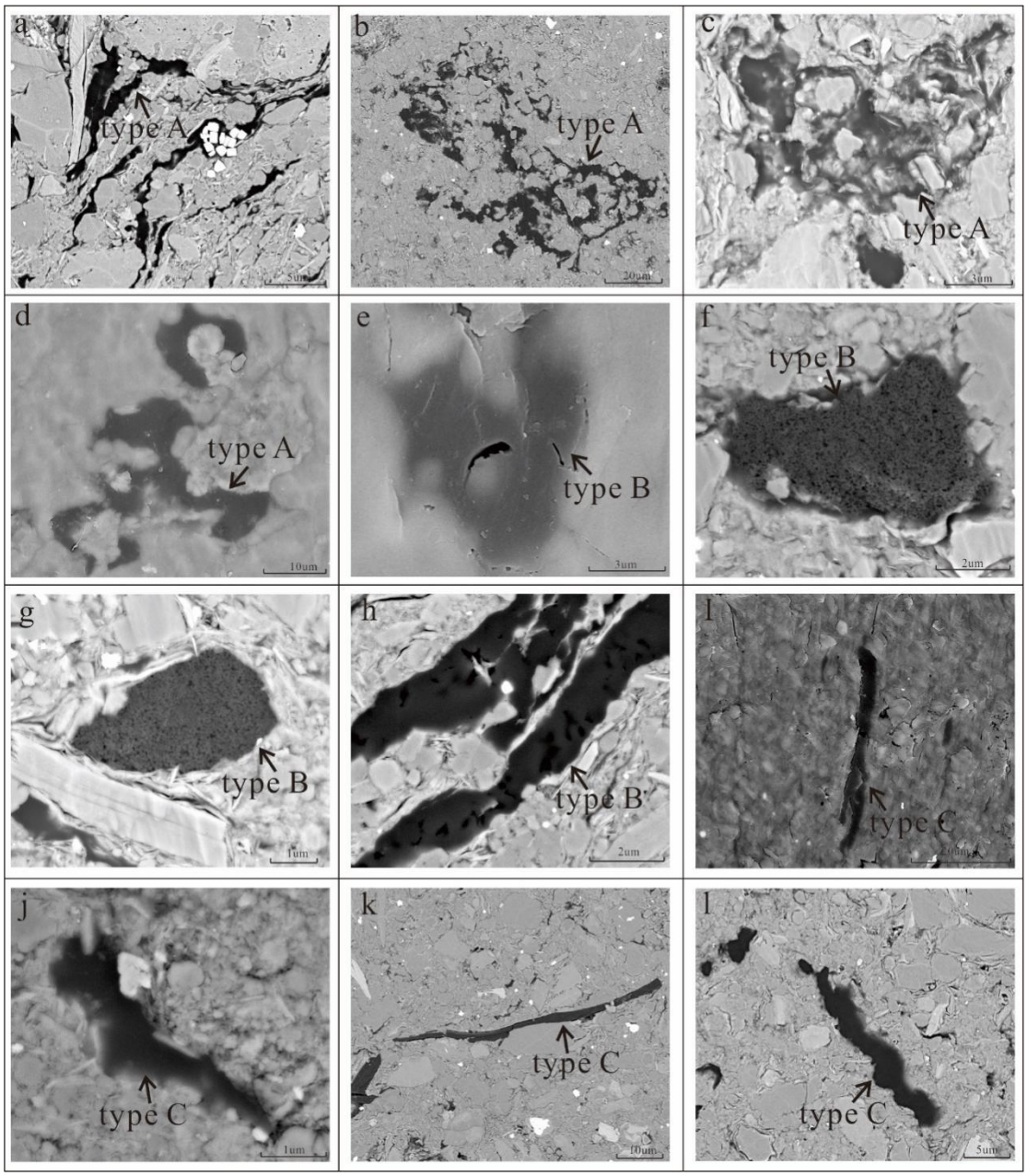

Fig. 5. Three types of organic pores in the Qingshankou shale from the southeastern uplift in the Songliao Basin.

The samples of picture a - c, f - h, j - l were collected from well ZK-36. a, h = 686 m; b, f, k = 736 m; c, g = 797 m; j = 775 m; l = 787 m. Other samples were collected from well ZK-36. d, e = 318 m; i = 349 m.

(2) Type B: The organic matter has intact bent strips or massive patterns and is mostly embedded in the matrix. The particles are always dozens of microns in size and contain abundant round, serrated, and honeycomb-shaped pores are developed with diameters of several dozens to hundreds of nanometers (Fig. 5e, f, g, h). Some interparticle pores are also developed on the edges of the organic matter.

(3) Type C: The organic matter is embedded in the matrix but has no obvious internal structure and

contains almost no porosity. Some interparticle pores are developed at the interfaces between organic matter and minerals such as clay and calcite (Fig. 5i, j, k, l). The organic matter is mainly bent strips and has large length–width ratios with sizes of dozens of microns. Some interparticle pores exist on the edges of organic matter.

Based on systematic observation of the morphology of the minerals, organic matter, and pores using SEM, clay pores, carbonate pores, organic pores, and pyrite pores were identified in the samples. Of these, the porosity of clay and carbonate contributed the most to total porosity, and few organic matter pores were developed (Fig. 4). Many pores formed within and on the edges of organic matter; therefore, type A and B organic matter had relatively high porosity (Fig. 5).

4.3 TOC content and mineral composition

The tested samples of shale were at a low-mature stage, and their average TOC content was 2.44%, with a minimum of 1.23% and a maximum of 4.82% (Table 2). According to the results of the XRD test, the main minerals in Qingshankou shale from the study area are clay, quartz, and feldspar. The average clay content of the shale is 51.9% with a minimum of 22.4% and a maximum of 73.1%. The contents of quartz + feldspar range from 9.3% to 41.0% with an average of 26.8% (Table 1). The contents of carbonate minerals such as calcite and dolomite have big differences between the samples; the maximum reached 59.7%. Compared with typical gas shale in North America (Chalmers et al., 2012), lacustrine shales of the 7th member of the Upper Triassic Yangchang Formation in the Ordos Basin (Yang et al., 2015a), and the mature to over-mature lower Silurian Longmaxi shale in southern China (Tian et al., 2013; Yang et al., 2015b; Zhang et al., 2015a), the low-maturity to mature Qingshankou shale contains more clay and less siliceous minerals in the study area, which makes it clay-rich (Fig 6). The main clay mineral is illite/smectite mixed layers, the content of which ranges from 62% to 95% with an average of 83.5%; and the mixed-layer ratio ranges from 33% to 40%. The illite content follows that of the mixed layer, and is between 5% and 29% with a mean of 13.4%; whereas the kaolinite and chlorite contents are rather small (Fig 7).

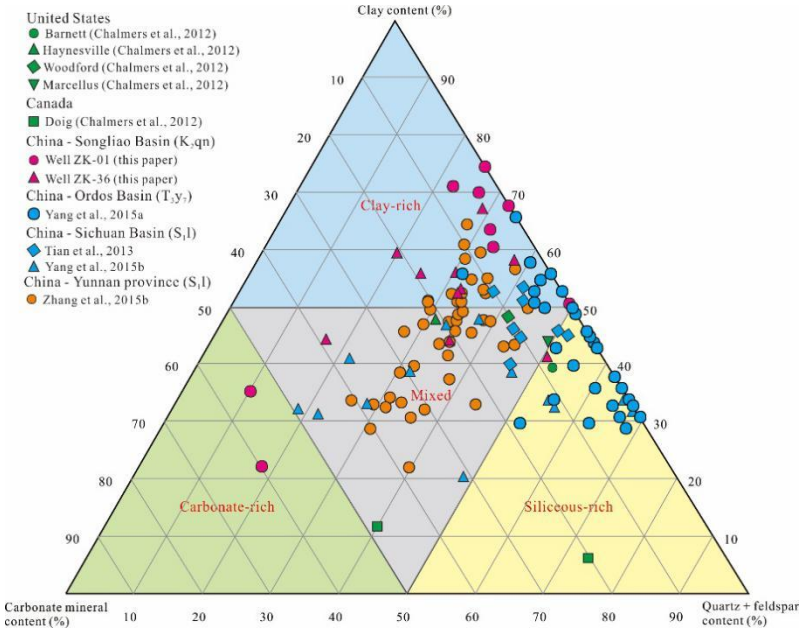

Fig. 6. Ternary diagram of mineral composition in the Qingshankou shale compared with other typical gas shales.

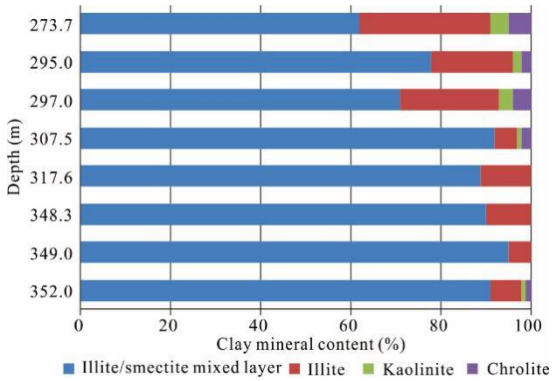

Fig. 7. Clay mineral contents of the Qingshankou shale collected from well ZK-01 in the southeastern uplift of the Songliao Basin.

5 Discussions

5.1 Factors influencing pore development

Vertically, with increasing depth, the TOC content and Ro of the samples increase, the carbonate minerals and clay mineral contents increase, and the content of quartz plus feldspar decreases in well ZK-36. For the samples, the average pore diameter increases, whereas the total pore volume and BET surface area have a downward trend (Fig. 8). Specifically, the contents of TOC and minerals as well as organic matter maturity play important roles in pore formation in the shale, which further influence hydrocarbon enrichment and preservation in the shale.

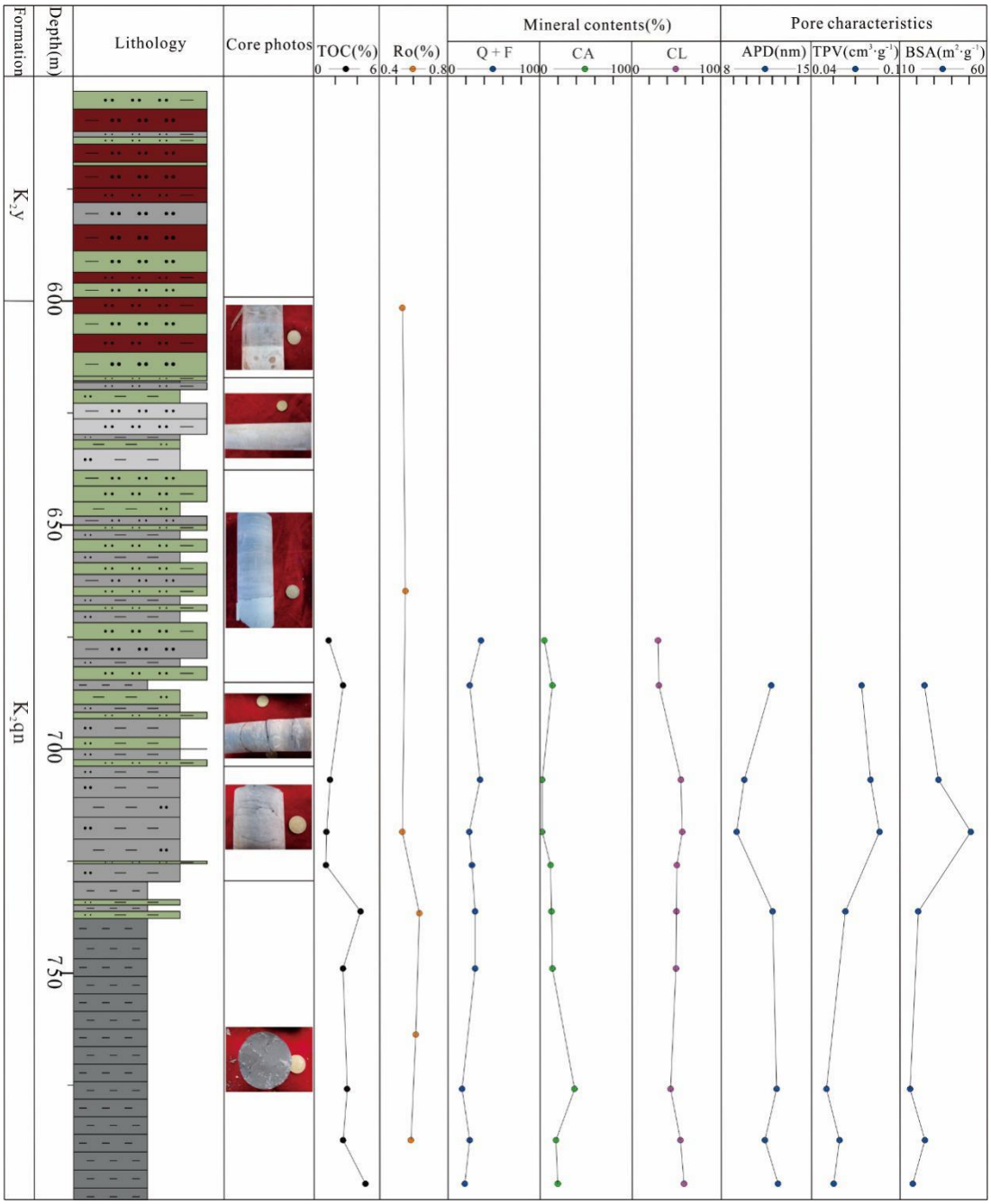

Fig. 8. Comprehensive stratigraphic column and the TOC, Ro, and mineral contents of the samples, and the pore characteristics for the Qingshankou Formation measured in well ZK-36.

Q + F = quartz plus feldspar. CA = carbonate minerals. CL = clay. APD = average pore diameter. TPV = total pore volume. BSA = BET surface area.

We further found that the TOC content of the samples had no clear relationship with total pore volume, but had a certain negative correlation with pore BET surface area (Fig. 9). Large pore volume is widely distributed in different scales of pores in the shale; however, pore surface area has an obvious negative linear correlation with average pore diameter (Fig. 10). Total pore volume development has some positive correlation with the contents of quartz + feldspar and clay; however, it has an apparent negative correlation with carbonate content. Pore surface area has a certain positive linear relationship with clay content and a negative correlation with carbonate content, whereas it has no prominent correlation with the content of quartz + feldspar (Fig. 11).

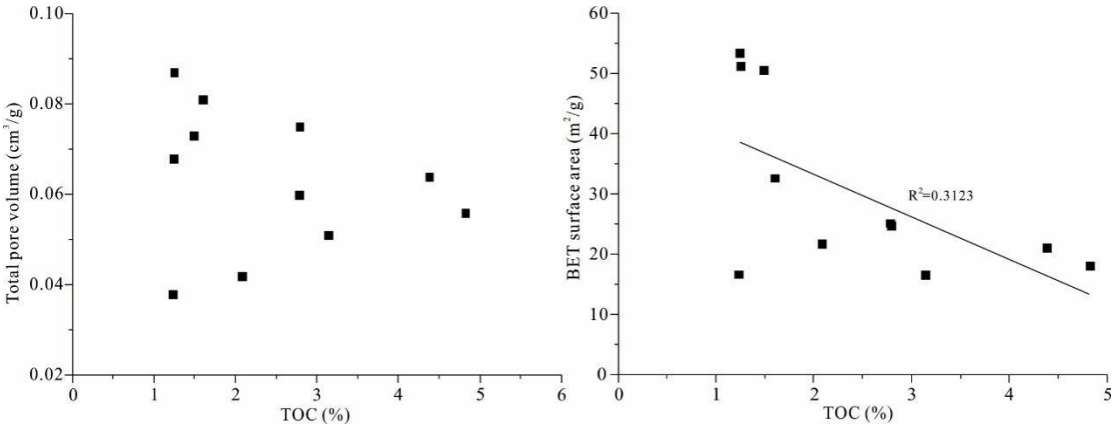

Fig. 9. Relationships of TOC content with total pore volume (left) and pore surface area (right) for the Qingshankou shale.

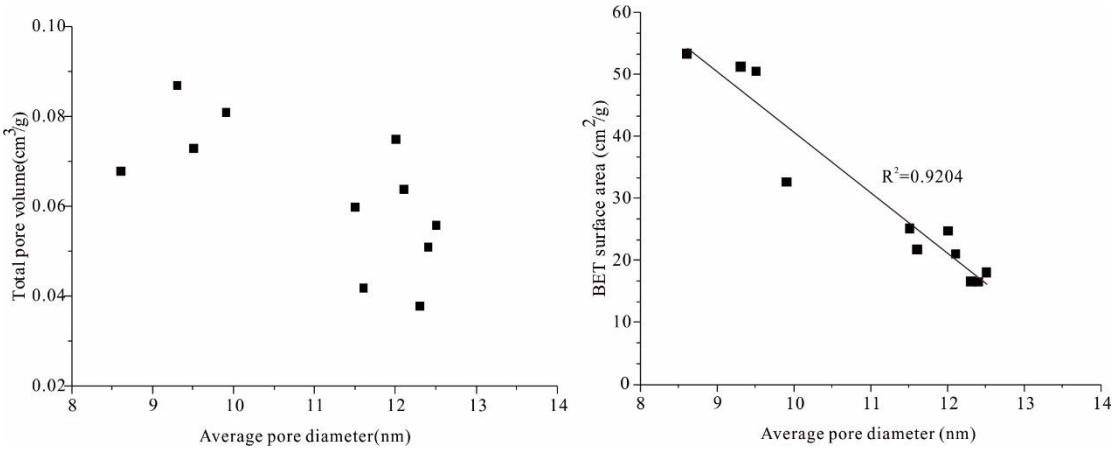

Fig. 10. Relationships of average pore diameter with total pore volume (left) and pore surface area (right) for the Qingshankou shale.

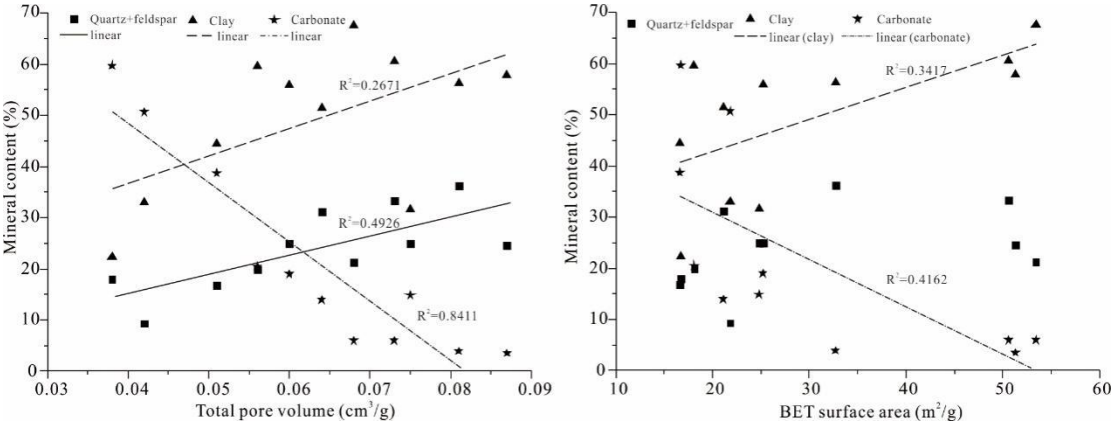

Fig. 11. Relationships of mineral contents with total pore volume (left) and pore surface area (right) for the Qingshankou shale.

5.2 Pore evolution

To observe the pore evolution characteristics with increasing maturity, we chose to heat samples

ZK-55 and ZK-68 at 380 ℃ and 460 ℃, respectively, for 48 hours. The two shale samples both have type Ⅰ organic matter and similar mineral compositions and maturity but different TOC contents of 1.25% and 2.78%, respectively. The results of the thermal simulation, shown in Table 3, indicate that the pore BET surface area decreased initially and then increased with increasing temperature. Relatively high-mature shale has lower pore surface area and greater total pore volume than the original low-mature shale (Fig. 12a, b). As the organic matter is gradually consumed, the average pore diameter obviously increases with increasing maturity (Fig. 12c). Relatively large pores contribute more to pore volume and inhibit the formation of pore surface areas. This case may represent a possible theory to explain the small increase in pore volume and decreasing surface area in the heated samples. Compared with the original shale, pores with diameters of less than 10 nm obviously decrease in the heated samples, but those with diameters of more than 10 nm contribute more to pore volume, and could comprise as much as 85% of the total pore volume (Fig. 13a, b, c). For the original shale with less micropore volume, like sample ZK-68, pores with diameters of less than 5 nm almost disappear in the heated samples, whereas pores with diameters of more than 10 nm contribute more than 90% of the total pore volume (Fig. 13d, e, f). What is interesting about the volume of pores with diameter of more than 10 nm is that it obviously increased during the preliminary heating stage, but decreased under relatively high temperature (Fig. 13). The N_2-GA adsorption–desorption isotherms of the samples all have narrow hysteresis loops, which are even narrower for the heated samples (Fig. 14). The pores in the heated samples present open shapes such as cylinders and are well connected. Compared with the original shale, which has fewer micropores (Fig. 15a, g, h), more carbonate mineral dissolution pores (Fig. 15b, d, e, i, j, k, l) and organic matter pores (Fig. 15c, f, i) were observed commonly in the heated samples. This result indicates that with the increasing maturity of the Qingshankou shale, many relatively large pores form in the organic matter, and the carbonate mineral pores become larger because of dissolution by organic acid, which makes the pores larger, more open, and more connected.

Based on the above description and analysis, we infer that in the initial stage of heating, the pores in the shale were dominated by original pores from organic matter and minerals, and micropores in the organic matter and clays contributed most to pore surface area. However, as maturity increased, carbonate minerals were continuously dissolved by organic acid from hydrocarbon generation, and many relatively large dissolution pores formed in the shale. When the illite/smectite mixed layer transformed to illite, the number of micropores in the layer decreased. Meanwhile, when the organic matter was continuously consumed, the TOC content of the shale decreased considerably, and many micropores formed within the organic matter.

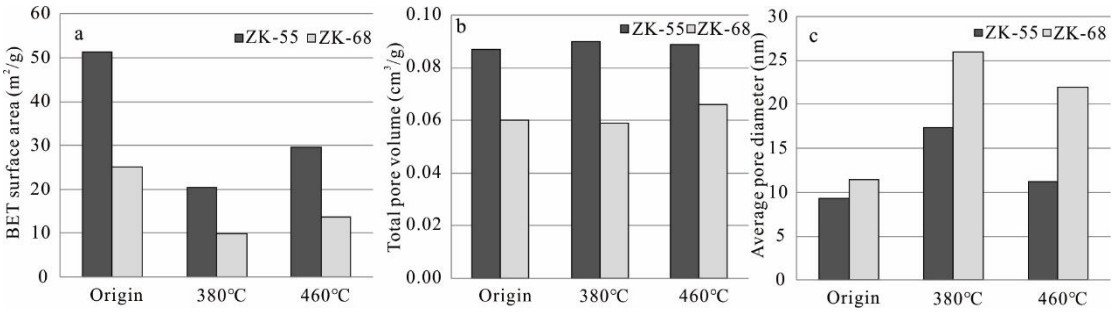

Fig. 12. Comparative results of pore surface area (a), total pore volume (b), and average pore diameter (c) of the Qingshankou shale.

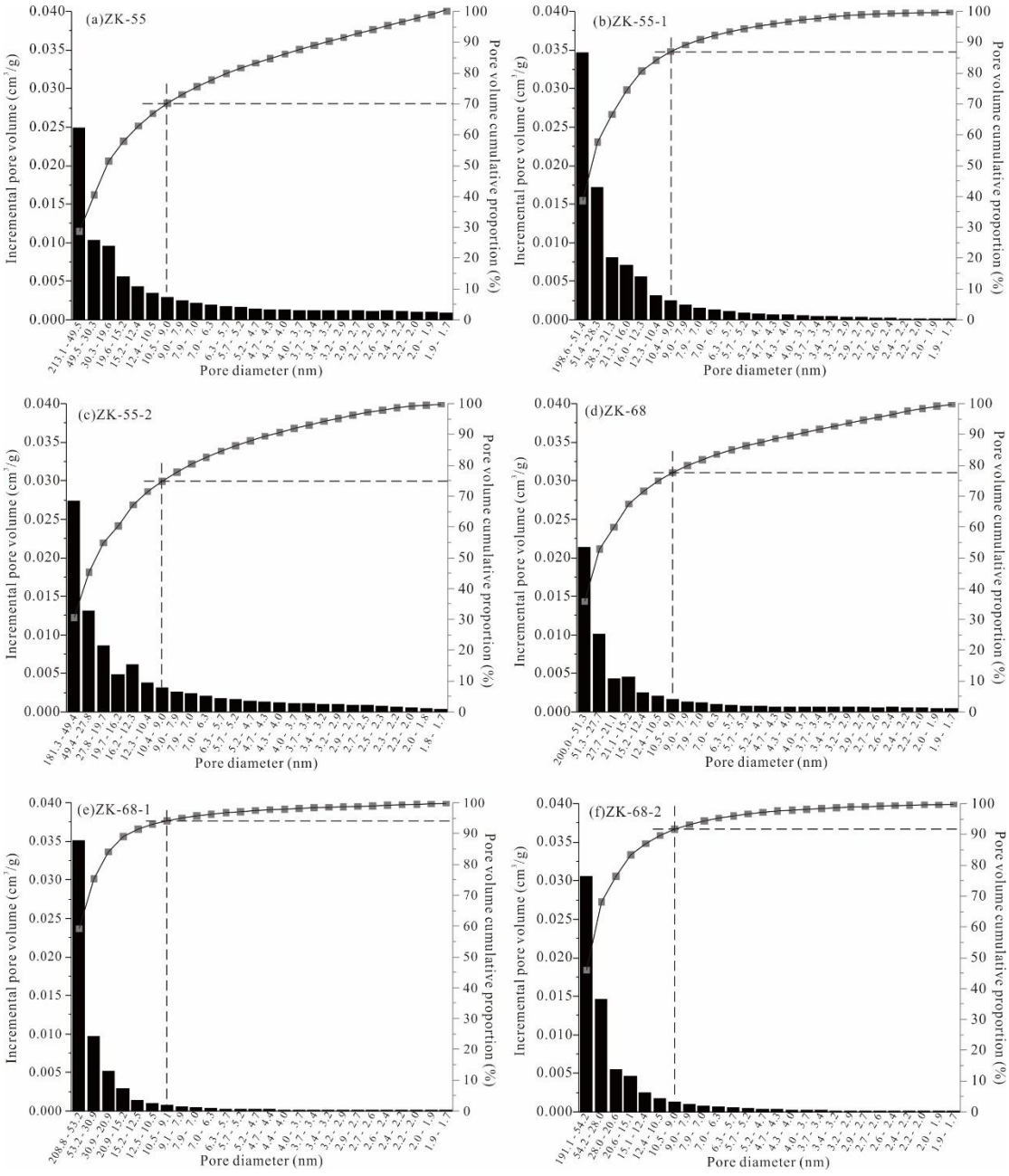

Fig. 13. Pore volume distribution and cumulative proportion of the Qingshankou shale and heated samples using N_2-GA.

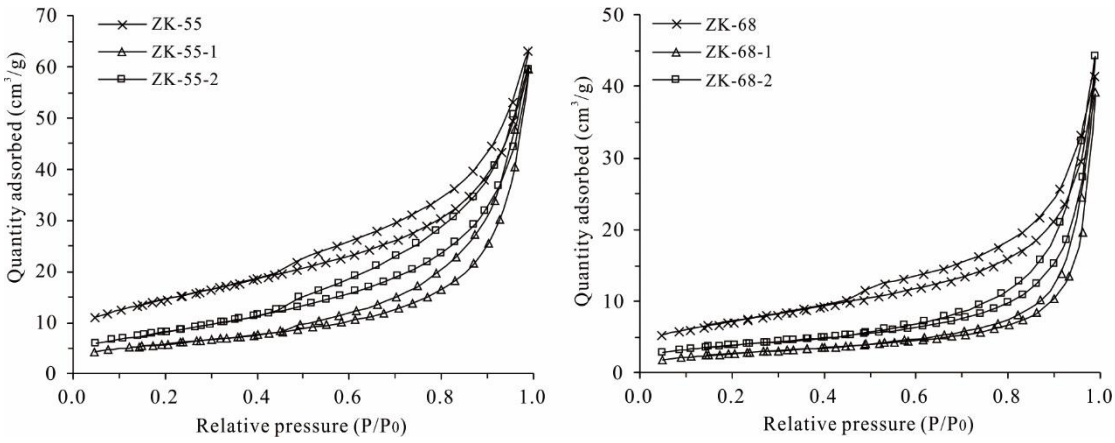

Fig. 14. Adsorption–desorption isotherms of the Qingshankou shale and heated samples using N_2-GA.

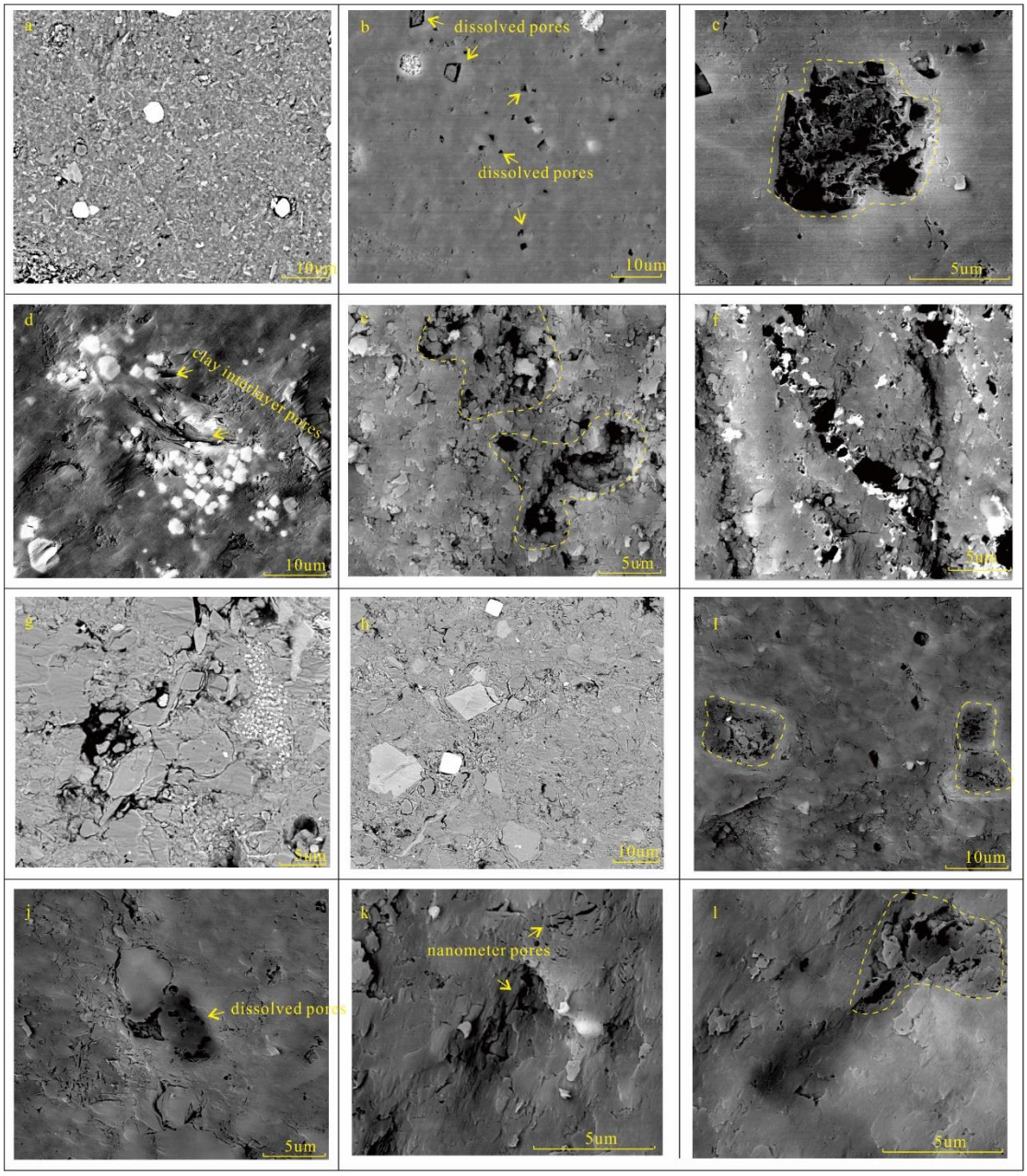

Fig. 15. Images of minerals and pores in the original and heated Qingshankou shale.

(a) ZK-55, original; (b) - (c) ZK-55-1, 380 ℃; (d) - (f) ZK-55-2, 460 ℃; (g) - (h) ZK-68, original; (i) - (j) ZK-68-1, 380 ℃; (k) - (l) ZK-68-2, 460 ℃.

6 Conclusions

(1) Mineral pores, especially clay and carbonate pores, contribute most to the porosity of the typical lacustrine Qingshankou shale. The organic matter pores are divided into types A, B, and C, among which the type B generates relatively high porosity in the shales.

(2) Pores with diameters of more than 10 nm account for the main component of pore volume in the shales, and most of the pores have half-open slit and wedge shapes. The total pore volume has no

obvious linear relationship with TOC content, but it has positive correlations with the contents of quartz + feldspar and clays, and a negative correlation with carbonate mineral content. The specific surface area of the pores has negative correlations with TOC content, average pore diameter, and carbonate mineral content, respectively; however, a positive correlation was found with clay content, and no clear linear relationship was found with quartz + feldspar content.

(3) The thermal simulation results show that carbonate mineral dissolution pores, organic matter pores, average pore diameter, and total pore volume increase with the increase of maturity in the lacustrine shales, but in contrast, the pore surface area decreases.

Acknowledgements

The authors sincerely thank the financial support of Special Scientific Research Project of Public Welfare Industry of Ministry of Land and Resources (Grant No.20121111051) and the National Natural Science Foundation of China (Grant No.41272159 and 41572099). This paper is also supported by Anhui Provincial Natural Science Foundation (Grant No.1908085MD105). We sincerely thank the editors and anonymous reviewers of Acta Geologica Sinica (English Edition) for their careful and instructive comments.

References

Bahadur, J., Melnichenko, Y.B., Mastalerz, M., Furmann, A., and Clarkson, C.R., 2014. Hierarchical pore morphology of Cretaceous shale: a small-angle neutron scattering and ultrasmall-angle neutron scattering study. *Energy & Fuels*, 28(10): 6336–6344.

Bahadur, J., Radlinski, A.P., Melnichenko, Y.B., Mastalerz, M., and Schimmelmann, A., 2015. Small-angle and ultrasmall-angle neutron scattering (SANS/USANS) study of New Albany shale: a treatise on microporosity. *Energy & Fuels*, 29(2): 567–576.

Bechtel, A., Jia, J.L., Strobl, S.A.I., Sachsenhofer, R.F., Liu, Z.J., Gratzer, R., and Puttmann, W., 2012. Paleoenvironmental conditions during deposition of the Upper Cretaceous oil shale sequences in the Songliao Basin (NE China): implications from geochemical analysis. *Organic Geochemistry*, 46: 76–95.

Brunauer, S., Deming, L.S., Deming, W.E., and Teller, E., 1940. On a theory of the van der Waals adsorption of gases. *Journal of the American Chemical Society*, 62: 1723–1732.

Chen, G.H., Lu, S.F., Li, J.B., Wang, W.M., Tian, S.S., Shan, J.F., Hu, Y.J., Mao, J.L., and HAN, X., 2015. The Oil-Bearing Pore Size Distribution of Lacustrine Shale from $E_2S_4^2$ Sub-Member in Damintun Sag, Liaohe Depression, Bohai Bay Basin, China. *Acta Geologica Sinica* (English Edition), 89(supp.): 8–10.

Chen, L., Jiang, Z.X., Liu, K.Y., Gao, F.L., and Wang, P.F., 2017. A combination of N_2 and CO_2 adsorption to characterize nanopore structure of organic-rich lower Silurian shale in the upper Yangtze Platform, south China: implications for shale gas sorption capacity. *Acta Geologica Sinica (English Edition)*, 91(4): 1380–1394.

Chen, S.B., Han, Y.F., Fu, C.Q., Zhang, H., Zhu, Y.M., and Zuo, Z.X., 2016. Micro and nano-size pores of clay minerals in shale reservoirs: Implication for the accumulation of shale gas. *Sedimentary Geology*, 342: 180–190.

Cao, T.T., Song, Z.G., Wang, S.B., and Xia, J., 2016. Characterization of pore structure and fractal dimension of Paleozoic shales from the northeastern Sichuan Basin, China. *Journal of Natural Gas Science and Engineering*, 35: 882–895.

Chalmers, G.R., Bustin, R.M., and Power, I.M., 2012. Characterization of gas shale pore systems by porosimetry, pycnometry, surface area, and field emission scanning electron microscopy/transmission electron microscopy image analyses: Examples from the Barnett, Woodford, Haynesville, Marcellus, and Doig units. *AAPG Bulletin*, 96: 1099–1119.

Clarkson, C.R., Haghshenas, B., Ghanizadeh, A., Qanbari, F., Williams-Kovacs, J.D., Riazi, N., Debuhr, C., and Deglint, H.J., 2016. Nanopores to megafractures: Current challenges and methods for shale gas reservoir and hydraulic fracture characterization. *Journal of Natural Gas Science and Engineering*, 31: 612–657.

Curtis, M.E., Cardott, B.J., Sondergeld, C.H., and Rai, C.S., 2012. Development of organic porosity in the Woodford Shale with increasing thermal maturity. *International Journal of Coal Geology*, 103: 26–31.

Dong, T., He, S., Yin, S.Y., Wang, D.X., Hou, Y.G., and Guo, J.G., 2015. Geochemical characterization of source rocks and crude oils in the Upper Cretaceous Qingshankou Formation, Changling Sag, southern Songliao Basin.

Marine Petroleum Geology, 64: 173–188.

Fishman, N.S., Hackley, P.C., Lowers, H.A., Hill, R.J., Egenhoff, S.O., Eberl, D.D., and Blum, A.E., 2012. The nature of porosity in organic-rich mudstones of the Upper Jurassic Kimmeridge Clay Formation, North Sea, offshore United Kingdom. *International Journal of Coal Geology*, 103: 32–50.

Gu, X., Cole, D.R., Rother, G., Mildner, D.F.R., and Barntley, S.L., 2015. Pores in Marcellus shale: a neutron scattering and FIB-SEM study. *Energy & Fuels*, 29(3): 1295–1308.

Guo Dongxing, 2012. *Regularity of mineralization and resources potential of oil shale of Qingshankou Formation in Songliao Basin*. Chinese University of Geosciences (Beijing) (Master thesis):1–50. (in Chinese with English abstract).

Guo, X.J., Shen, Y.H., and He, S.L., 2015. Quantitative pore characterization and the relationship between pore distributions and organic matter in shale based on Nano-CT image analysis: A case study for a lacustrine shale reservoir in the Triassic Chang 7 member, Ordos Basin, China. *Journal of Natural Gas Science and Engineering*, 27: 1630–1640.

Han, H., Liu, P.W., Ding, Z.G., Shi, P.T., Jia, J.C., Zhang, W., Liu, Y., Chen, S.J., Lu, J.G., Chen, K., Peng, X.D., Wang, Z.Y., Xiao, S.Q., and Gao, Y., 2018. The influence of extractable organic matter on pore development in the late Triassic Chang 7 lacustrine shales, Yanchang Formation, Ordos Basin, China. *Acta Geologica Sinica* (English Edition), 92(4): 1508–1522.

Hao, Z.G., Fei, H.C., Hao, Q.Q., and Liu, L., 2017. China's shale gas geological investigation and prospecting have made significant progress. *Acta Geologica Sinica* (English Edition), 91(2): 727–728.

Huang, W.B., Deng, S.W., Lu, S.F., Yu, L., Hu, S., and Zhang, J., 2014. Shale organic heterogeneity evaluation method and its application to shale oil resource evaluation: a case study from Qingshankou Formation, southern Songliao Basin. *Oil & Gas Geology*, 35(5): 704–711 (in Chinese with English abstract).

Huang, Z.K., Chen, J.P., Wang, Y.J., Xue, H.T., Deng, C.P., and Wang, M., 2013a. Characteristics of micropores in mudstones of the Cretaceous Qingshankou Formation, Songliao Basin. *Acta Petrolei Sinica*, 34(1): 31–35. (in Chinese with English abstract).

Huang, Z.K., Chen, J.P., Wang, Y.J., Deng, C.P., and Xue, H.T., 2013b. Pore distribution of source rocks as revealed by gas adsorption and mercury injection methods: a case study on the first member of the Cretaceous Qingshankou Formation in the Songliao Basin. *Geological Review*, 59(3): 587–594. (in Chinese with English abstract).

Huo, Q.L., Zeng, H.S., Zhang, X.C., and Fu, L., 2012. An evaluation diagram of effective source rocks in the first member of Qingshankou Formation in northern Songliao Basin and its implication. *Acta Petrolei Sinica*, 33(3): 379–384. (in Chinese with English abstract).

Jarvie, D.M., Hill, R.J., Ruble, T.E., and Pollastro, R.M., 2007. Unconventional shale-gas systems: the Mississippian Barnett Shale of north-central Texas as one model for thermogenic shale-gas assessment. *AAPG Bulletin*, 91: 475–499.

Jiang, Z.X., Zhang, W.Z., Liang, C., Wang, Y.S., Liu, H.M., and Chen, X., 2014. Characteristics and evaluation elements of shale oil reservoir. *Acta Petrolei Sinica*, 35(1): 184–196. (in Chinese with English abstract).

King, Jr.H.E., Eberle, A.P.R., Walters, C.C., Kliewer, C.E., Ertas, D., and Huynh, C., 2015. Pore architecture and connectivity in gas shale. *Energy & Fuels*, 29(3): 1375–1390.

Klaver, J., Desbois, G., Urai, J.L., and Littke, R., 2012. BIB-SEM study of the pore space morphology in early mature Posidonia Shale from the Hils area, Germany. *International Journal of Coal Geology*, 103: 12–25.

Klaver, J., Desbois, G., Littke, R., and Urai, J.L., 2015. BIB-SEM characterization of pore space morphology and distribution in postmature to overmature samples from the Haynesville and Bossier Shales. *Marine and Petroleum Geology*, 59: 451–466.

Labani, M.M., Rezaee, R., Saeedi, A., and Hinai, A.A., 2013. Evaluation of pore size spectrum of gas shale reservoirs using low pressure nitrogen adsorption, gas expansion and mercury porosimetry: A case study from the Perth and Canning Basins, Western Australia. *Journal of Petroleum Science and Engineering*, 112: 7–16.

Li, Z.D., Wang, Y.J., Hu, H.T., Wang, H.S., Zhang, H.X., Li, Y., and Zhu, X.M., 2015. Shale reservoir characteristics of Qing-1 member of Cretaceous Qingshankou Formation in Northern Songliao Basin. *Xinjiang Petroleum Geology*, 36(1): 20–24. (in Chinese with English abstract).

Liu, C.L., Ma, Y.S., Zhou, G., Yin, C.M., Du, J.J., Gong, W.B., Fan, T.Y., Liu, W.P., Xu, Y., and Zhang, Q., 2012. Evidence for the Carboniferous hydrocarbon generation in Qaidam Basin. *Acta Petrolei Sinica*, 33(6): 1–7. (in Chinese with English abstract).

Liu, Z.J., Sun, P.C., Liu, R., Meng, Q.T., Bai, Y.Y., and Xu, Y.B., 2014a. Research on Geological Conditions of Shale Coexistent Energy Mineralization (Accumulation): Take the Qingshankou Formation in Upper Cretaceous, Songliao Basin for example. *Acta Sedimentological Sinica*, 32(3): 593–600. (in Chinese with English abstract).

Liu, B., Lv, Y.F., Ran, Q.C., Dai, C.L., Li, M., and Wang, M., 2014b. Geological conditions and exploration potential of shale oil in Qingshankou Formation, Northern Songliao Basin. *Oil & Gas Geology*, 35(2): 280–285. (in Chinese with English abstract).

Loucks, R.G. and Ruppel, S.C., 2007. Mississippian Barnett shale: lithofacies and depositional setting of a deep-water shale-gas succession in the Fort Worth Basin, Texas. *AAPG Bulletin*, 91(4): 579–601.

Loucks, R.G., Reed, R.M., Ruppel, S.C, and Hammes, U., 2012. Spectrum of pore types and networks in mudrocks and a descriptive classification for matrix-related mudrock pores. *AAPG Bulletin*, 96(6): 1071–1098.

Mastalerz, M., He, L.L., Melnichenko, Y.B., and Rupp, J.A., 2012. Porosity of coal and shale: insights from gas adsorption and SANS/USANS techniques. *Energy & Fuels*, 26(8): 5109–5120.

Ran, B., Liu, S.G., Luba Jansa, Sun, W., Yang, D., Wang, S.Y., Ye, Y.H., Christopher Xiao, Zhang, J., Zhai, C.B., Luo, C., and Zhang, C.J., 2016. Reservoir characteristics and preservation conditions of Longmaxi shale in the upper Yangtze block, south China. *Acta Geologica Sinica (English Edition)*, 90(6): 2182–2205.

Shu, L.S., Mu, Y.F., and Wang, B.C., 2003. The Oil-Gas-Bearing strata and the structural features in the Songliao Basin, NE China. *Journal of Stratigraphy*, 27(4): 340–347. (in Chinese with English abstract).

Slatt, R.M., and O'Brien, N.R., 2011. Pore types in the Barnett and Woodford gas shales: contribution to understanding gas storage and migration pathways in fine–grained rocks. *AAPG Bulletin*, 95(12): 2017–2030.

Suárez-Ruiz, I., Juliao, T., Suárez-García, F., Marquez, R., and Ruiz, B., 2016. Porosity development and the influence of pore size on the CH_4 adsorption capacity of a shale oil reservoir (Upper Cretaceous) from Colombia. Role of solid bitumen. *International Journal of Coal Geology*, 159: 1–17.

Tian, H., Pan, L., Xiao, X.M., Wilkins, R.W.T., Meng, Z.P., and Huang, B.J., 2013. A preliminary study on the pore characterization of Lower Silurian black shales in the Chuandong Thrust Fold Belt, southwestern China using low pressure N_2 adsorption and FE–SEM methods. *Marine and Petroleum Geology*, 48: 8–19.

Wang, C.S., Feng, Z.Q., Zhang, L.M., Huang, Y.J., Cao, K., Wang, P.J., and Zhao, B., 2013. Cretaceous paleogeography and paleoclimate and the setting of SKI borehole sites in Songliao Basin, northeast China. *Palaeogeography, Palaeoclimatology, Palaeoecology*, 385: 17–30.

Wang, Y., Zhu, Y.M., Chen, S.B., and Li, W., 2014. Characteristics of the nanoscale pore structure in northwestern Hunan shale gas reservoirs using field emission scanning electron microscopy, high-pressure mercury intrusion, and gas adsorption. *Energy & Fuels*, 28: 945–955.

Wang, M., Yang, J.X., Wang, Z.W., and Lu, S.F., 2015. Nanometer-scale pore characteristics of lacustrine shale, Songliao Basin, NE China. *PLoS ONE*, 10(8), e0135252. doi:10.1371/journal.pone.0135252.

Wang, M., Lu, S.F., Wang, Z.W., Liu, Y., Huang, W.B., Chen, F.W., Xu, X.Y., Li, Z., and Li, J.J., 2016a. Reservoir characteristics of lacustrine shale and marine shale: examples from the Songliao Basin, Bohai Bay Basin and Qiannan depression. *Acta Geologica Sinica (English Edition)*, 90(3): 1024–1038.

Wang, P.F., Jiang, Z.X., Yin, L.S., Chen, L., Li, Z., Zhang, C., Li, T.W., and Huang, P., 2017. Lithofacies classification and its effect on pore structure of the Cambrian marine shale in the Upper Yangtze Platform, South China: Evidence from FE-SEM and gas adsorption analysis. *Journal of Petroleum Science and Engineering*, 156: 307–321.

Wang, Y., Zhu, Y.M., Liu, S.M., and Zhang, R., 2016b. Pore characterization and its impact on methane adsorption capacity for organic-rich marine shales. *Fuel*, 181: 227–237.

Xue, H.Q., Jiang, P.X., Xu, R.N., Zhao, B., and Zhou, S.W., 2016. Characterization of the reservoir in Lower Silurian and Lower Cambrian shale of south Sichuan Basin, China. *Journal of Natural Gas Science and Engineering*, 29: 150–159.

Yang, Y.T., Liang, C., Zhang, J.C., Jiang, Z.X., and Tang, X., 2015a. A developmental model of lacustrine shale gas genesis: A case from T_3y^7 shale in the Ordos Basin, China. *Journal of Natural Gas Science and Engineering*, 22: 295–405.

Yang, F., Ning, Z.F., Zhang, R., Zhao, H.W., and Krooss, B.M., 2015b. Investigations on the methane sorption capacity of marine shales from Sichuan Basin, China. *International Journal of Coal Geology*, 146: 104–117.

Yang, F., Ning, Z.F., Wang, Q., and Liu, H.Q., 2016. Pore structure of Cambrian shales from the Sichuan Basin in China and implications to gas storage. *Marine and Petroleum Geology*, 70: 14–26.

Zhai, G.M., and Ding, Z.Y., 1993. *Petroleum geology of China* (Vol.2). Beijing: Petroleum Industry Press. (in Chinese).

Zhang, X., Liu, C.L., Zhu, Y.M., Wang, Y., and Fu, C.Q., 2015. Geological conditions evaluation and favorable area selection of the shale gas from Longmaxi Formation in the northeast of Yunnan. *Natural Gas Geoscience*, 26(6): 1190–1199. (in Chinese with English abstract).

Zhang, X., Liu, C.L., Zhu, Y.M., Chen, S.B., Wang, Y., and Fu, C.Q., 2015a. The characterization of a marine shale gas reservoir in the lower Silurian Longmaxi Formation of the northeastern Yunnan Province, China. *Journal of Natural Gas Science and Engineering*, 27: 321–335.

Zhang, J.P., Fan, T.L., Li, J., Zhang, J.C., Li, Y.F., Wu, Y., and Xiong, W.W., 2015b. Characterization of the lower Cambrian shale in the northwestern Guizhou province, south China: implications for shale–gas potential. *Energy & Fuels*, 29(10): 6383–6393.

Zhuo, H.C., Lin, C.M., Li, Y.L., Feng, Z.Q., Zhang, S., and Zhao, B., 2007. Characteristics of sedimentary facies and sequence boundary in upper Cretaceous Qingshankou-Yaojia Formation of northern Songliao Basin. *Acta Sedimentologica Sinica*, 25(1): 29–38. (in Chinese with English abstract).

About the first author

ZHANG Xu, male, born in 1990 in Chaohu City, Anhui Province; Ph.D.; graduated from Chinese Academy of Geological Science; a postdoctor of University of Science and Technology of China, and an engineer of Geological Exploration Technology Institute of Anhui Province. He is now interested in the study on unconventional oil and gas geology. Email: xuzhangcags@163.com

About the corresponding author

1. LIU Chenglin, male, born in 1970 in Ziyang City, Sichuan Province; Ph.D.; graduated from China University of Petroleum, Beijing; a professor of college of geosciences, China University of Petroleum, Beijing. He is now interested in the study on oil and gas resources evaluation. Email: liucl@cup.edu.cn. 2. GUI Herong, male, born in 1963 in Liu'an City, Anhui Province; Ph.D.; graduated from University of Science and Technology of China; a professor of National Engineering Research Center of Coal Mine Water Hazard Controlling (Suzhou University). He is now interested in the study on coal geology and hydrogeology. Email: hrgui@163.com.

Table 1 Mineral contents of the Upper Cretaceous Qingshankou mudstone and shale in the southeastern uplift of the Songliao Basin.

Sample number		Depth (m)	Mineral content (%) [a]															Clay mineral relative contents (%)				
			Qua	Pla	Cal	Pyr	Ana	Bar	Gyp	Pyr	Dol	Ank	Sid	Hem	Cla	Q+F	CA	Others	I/S	I	K	C	Ratio
Well ZK-01	SL-10	273.7	29.9	11.1	0.0	0.0	7.8	8.7	0.0	0.0	0.0	0.0	0.0	0.0	42.5	41.0	0.0	16.5	62.0	29.0	4.0	5.0	33
	SL-9	295.0	27.1	6.2	6.0	0.0	0.0	0.0	0.0	0.0	0.0	0.0	0.0	0.0	60.6	33.3	6.0	0.1	78.0	18.0	2.0	2.0	35
	SL-8	297.0	20.1	6.5	3.2	0.0	0.0	0.0	0.0	0.0	0.0	0.0	0.0	0.0	70.2	26.6	3.2	0.0	71.0	22.0	3.0	4.0	40
	SL-6	307.5	9.3	0	50.7	7.0	0.0	0.0	0.0	0.0	0.0	0.0	0.0	0.0	33.0	9.3	50.7	7.0	92.0	5.0	1.0	2.0	40
	SL-5	317.6	13.5	7.7	6.0	5.2	0.0	0.0	0.0	0.0	0.0	0.0	0.0	0.0	67.6	21.2	6.0	5.2	89.0	11.0	0.0	0.0	35
	SL-4	339.9	23.7	7.3	4.8	0.0	0.0	0.0	1.0	0.0	0.0	0.0	0.0	0.0	63.2	31.0	4.8	1.0	NA	NA	NA	NA	NA
	SL-3	348.3	18.0	6.8	0.0	2.1	0.0	0.0	0.0	0.0	0.0	0.0	0.0	0.0	73.1	24.8	0.0	2.1	90.0	10.0	0.0	0.0	33
	SL-2	349.0	15.7	2.2	0.0	0.0	0.0	0.0	0.0	0.0	59.7	0.0	0.0	0.0	22.4	17.9	59.7	0.0	95.0	5.0	0.0	0.0	33
	SL-1	352.0	23.0	7.1	0.0	0.0	0.0	0.0	0.0	6.2	0.0	0.0	0.0	0.0	63.7	30.1	0.0	6.2	91.0	7.0	1.0	1.0	40
Well ZK-36	ZK-49	675.7	26.7	10.7	3.7	0.0	22.4	0.0	0.0	0.0	0.0	0.0	2.3	3.5	30.7	37.4	6.0	25.9	NA	NA	NA	NA	NA
	ZK-50	685.7	16.2	8.8	0.0	3.2	17.3	0.0	0.0	4.6	0.0	12.6	2.3	3.2	31.7	25.0	14.9	28.4	NA	NA	NA	NA	NA
	ZK-53	706.7	24.2	12.1	3.9	3.4	0.0	0.0	0.0	0.0	0.0	0.0	0.0	0.0	56.3	36.3	3.9	3.5	NA	NA	NA	NA	NA
	ZK-55	718.3	16.8	7.7	3.5	3.4	9.0	0.0	0.0	0.0	0.0	0.0	0.0	1.7	57.9	24.5	3.5	14.1	NA	NA	NA	NA	NA
	ZK-57	725.7	18.4	9.3	3.4	2.8	5.0	0.0	0.0	0.0	0.0	9.3	0.0	0.0	51.7	27.7	12.7	7.9	NA	NA	NA	NA	NA
	ZK-60	736.0	20.8	10.3	3.6	3.6	0.0	0.0	0.0	0.0	0.0	10.4	0.0	0.0	51.4	31.1	14.0	3.5	NA	NA	NA	NA	NA
	ZK-62	748.7	23.2	7.6	11.4	3.8	0.0	0.0	0.0	0.0	0.0	0.0	3.4	0.0	50.6	30.8	14.8	3.8	NA	NA	NA	NA	NA
	ZK-66	775.5	12.4	4.4	0.0	0.0	0.0	0.0	0.0	0.0	38.7	0.0	0.0	0.0	44.5	16.8	38.7	0.0	NA	NA	NA	NA	NA
	ZK-68	786.9	18.3	6.7	0.0	0.0	0.0	0.0	0.0	0.0	15.4	0.0	3.6	0.0	56.0	25.0	19.0	0.0	NA	NA	NA	NA	NA

ZK-70	796.6	13.7	6.2	6.0	0.0	0.0	0.0	0.0	0.0	14.5	0.0	0.0	0.0	59.6	19.9	20.5	0.0	NA	NA	NA	NA	NA

[a] Tested by using X-ray diffraction, Qua = quartz, Pla = plagioclase, Cal = calcite, Pyr = pyrite, Ana = analcite, Bar = barite, Gyp = gypsum, Pyr = pyroxene, Dol = dolomite, Ank = ankerite, Sid = siderite, Hem = hematite, Cla = clay, Q + F = quartz + feldspar, CA = carbonate, I/S = illite/smectite mixed layer, I = illite, K = kaolinite, C = chlorite, Ratio = illite/smectite mixed layer ratio (S%). [b] Illite + Kaolinite + Chlorite + mixed Illitite/smectite layer = clay minerals 100%. [c] NA = not applicable.

Table 2 Minerals content, TOC content, vitrinite reflectance, and pore characteristics of the Qingshankou shale in the study area.

Sample number		Main mineral contents (%)			TOC (%)	R_o (%)	N_2-GA		
		Quartz+ feldspar	Carbonate	Clay			BET surface area(m^2/g)	Average pore diameter(nm)	Total pore volume(cm^3/g)
well ZK-01	SL-2	17.9	59.7	22.4	1.23	0.68	16.7	12.3	0.038
	SL-5	21.2	6.0	67.6	1.24	0.57	53.4	8.6	0.068
	SL-6	9.3	50.7	33.0	2.08	0.69	21.8	11.6	0.042
	SL-9	33.3	6.0	60.6	1.49	0.83	50.6	9.5	0.073
well ZK-36	ZK-50	25.0	14.9	31.7	2.79	0.51	24.8	12.0	0.075
	ZK-53	36.3	3.9	56.3	1.60	NA [a]	32.7	9.9	0.081
	ZK-55	24.5	3.5	57.9	1.25	0.54	51.3	9.3	0.087
	ZK-60	31.1	14.0	51.4	4.38	0.64	21.1	12.1	0.064
	ZK-66	16.8	38.7	44.5	3.14	0.61	16.6	12.4	0.051
	ZK-68	25.0	19.0	56.0	2.78	0.59	25.2	11.5	0.060
	ZK-70	19.9	20.5	59.6	4.82	NA	18.1	12.5	0.056

[a] NA = not applicable.

Table 3 Thermal evolution results for the Qingshankou shale in the Songliao Basin.

Sample number	Formation	Temperature (time)	N_2-GA		
			BET surface area (m^2/g)	BJH total pore volume (cm^3/g)	Average pore diameter (nm)
ZK-55	Qingshankou (K_2qn)	Original rock	51.3	0.087	9.3
ZK-55-1		380℃(48h)	20.5	0.090	17.4
ZK-55-2		460℃(48h)	29.6	0.089	11.2
ZK-68		Original rock	25.2	0.060	11.5
ZK-68-1		380℃(48h)	9.8	0.059	26.0
ZK-68-2		460℃(48h)	13.7	0.066	21.9